

Finsler geometry modeling of phase separation in multi-component membranes

Satoshi Usui and Hiroshi Koibuchi

National Institute of Technology, Ibaraki College
Nakane 866, Hitachinaka, Ibaraki 312-8508, Japan

Abstract. Finsler geometric surface model is studied as a coarse-grained model for membranes of three-component such as DOPC, DPPC and Cholesterol. To understand the phase separation of liquid ordered (DPPC rich) L_o and the liquid disordered (DOPC rich) L_d , we introduce a variable $\sigma(\in \{1, -1\})$ in the triangulated surface model. We numerically find that there appear two circulars and stripe domains on the surface and that these two morphologies are separated by a phase transition. The morphological change from the one to the other with respect to the variation of the area fraction of L_o is consistent with existing experimental results. This gives us a clear understanding of the origin of the line tension energy, which has been used to understand those morphological changes in the three-component membranes. In addition to these two circulars and stripe domains, raft-like domain and budding domain are also observed, and the corresponding several phase diagrams are obtained. Technical details of the Finsler geometry modeling are also shown.

1. Introduction

Membranes of multi-component such as DOPC, DPPC and Cholesterol are getting broad attention because of the applications in many fields of sciences and technologies, and a lot of studies on the morphological changes have been conducted [1, 2, 3, 4, 5, 6]. In those membranes, the morphological changes are induced by a phase separation. Indeed, the phase separation causes the domain formation and the domain pattern transition between the liquid-ordered (L_o) and the liquid-disordered (L_d) phases. This domain pattern transition accompanies the change of morphologies such as the two circulars domain, the stripe domain, the raft domain and the so-called budding domain [5, 6]. Multiplicity of components, just like in a glass transition [7], is essential for such a variety of morphologies. Up to now, these morphologies have been studied on the basis of the line tension energy [3, 4] in the context of Helfrich-Polyakov (HP) model for membranes [8, 9, 10]. However, the origin of the line tension energy is not well understood.

Therefore, in this paper we clarify and understand the microscopic origin of the line tension energy. The line tension energy is defined on the domain boundary and has an important role for the morphological changes [3, 4]. However, the problem that should be asked is where the line tension energy comes from. In fact, it is unclear what kind of internal structure is connected to the line tension energy until now.

To understand the origin of the line tension energy, we use Finsler geometry (FG) model, which is constructed by extending the HP model [11]. We emphasize that general HP model, where "general" HP model means the HP model with a nontrivial surface metric $g_{ab}(\neq \delta_{ab})$, can be discretized on triangulated surfaces and becomes well defined only when it is treated in the context of Finsler geometry [11, 12, 13]. Another feature of the FG model is that the Hamiltonian is not symmetric under the change of surface orientation, where the change of orientation for a sphere is realized by turning the sphere inside out. We should note that such a change of the configuration can be observed in cells as the inversion [14]. It is also expected, in the so-called buckling phenomenon [15], that the surfaces with two different orientations are observed in a cup like membrane [16, 17]. The energy difference between these two configuration is expected in the context of FG modeling. However, no such energy difference is expected in the model of this paper, because the model in this paper is orientation symmetric. The reason why the model is orientation symmetric, even though it is obtained from the orientation asymmetric FG model, is because it is obtained by a certain simplification, which is suitable to study multi-component membranes. Nevertheless, the model in this paper is meaningful and non-trivial because it is well defined only in the context of Finsler geometry as mentioned above.

This paper is organized as follows: In Section 2, we describe the technical details of the FG modeling for readers who are interested in the modeling. Readers who are not interested in the modeling itself can skip Section 2 and start with Section 3. In Subsection 2.1, we introduce the continuous Hamiltonian, which is identical to the Polyakov action for rigid string model [9] except the difference between the Finsler

metric $g_{ab}(x, y)$ and Riemannian metric $g_{ab}(x)$. The discretization of this continuous model on the triangulated surfaces is described in 2.2, and a discrete model is obtained. From this discrete model, we have the simplified discrete model by imposing a constraint on the metric function. In 2.3, we discuss the orientation symmetry, and we show that both the first and the second models are ill-defined in the conventional modeling on triangulated surfaces. It is also shown that the models turn to be well defined in the context of Finsler geometry. In 2.4, we briefly describe how to construct the FG surface model starting with a discrete Finsler function defined on the triangulated surfaces. In Section 3, we introduce the two components surface model, which is defined by including aggregation energy into the Hamiltonian of the FG surface model constructed in Section 2. The aggregation energy is defined by the variable σ , which is introduced to label the triangles with L_o and L_d . Monte Carlo technique is briefly shown in Section 4, and the MC results are presented in Section 5. Finally, we summarize the results in Section 6.

2. Surface model

2.1. Continuous surface model

We start with a continuous surface model, which is defined by the Polyakov action S_1 for string model and the extrinsic curvature action S_2 with a Finsler metric $g(x, y)$, where $x=(x_1, x_2)$ and $y(=\dot{x})$ are the local coordinate of M and its derivative [18]. Both of the energies are closely connected to the mapping X from M to \mathbf{R}^3 and are given by

$$S_1 = \int \sqrt{g} d^2x g^{ab} \frac{\partial X^\mu}{\partial x_a} \frac{\partial X^\mu}{\partial x_b}, \quad S_2 = \frac{1}{2} \int \sqrt{g} d^2x g^{ab} \frac{\partial n^\mu}{\partial x_a} \frac{\partial n^\mu}{\partial x_b}, \quad (1)$$

where g is the determinant of the 2×2 matrix g_{ab} of metric function, and g^{ab} is its inverse [18]. The symbol n^μ ($\mu=1, 2, 3$) denotes a unit normal vector of the surface, and $\partial_a n^\mu \partial_b n^\mu$ is the first fundamental form of the Gauss's sphere. Both S_1 and S_2 are conformally invariant and reparametrization invariant. The reparametrization invariance is limited only for the models where g_{ab} is independent of y [11]. The conformal invariance is a property in which a scale change $g_{ab}(x, y) \rightarrow f(x)g_{ab}(x, y)$ in M is not reflected in both S_1 and S_2 for any positive function f on M . This is a local scale invariance in M for S_1 and S_2 . Two metrics g and g' are called "conformally equivalent" if there exists a function $f(x)$ such that $g'_{ab} = f(x)g_{ab}$ [18]. The idea of strings, which sweep out the world sheet, is originated by Nambu [19].

For the case that $g_{ab}(x)$ depends only on x , both the surface shape $X(M)$ in \mathbf{R}^3 and the metric g on M are treated from the point of view of statistical mechanics. These are the HP model [8, 9, 10] and the Landau-Ginzburg model [20] for membranes, and the models have been thoroughly investigated [21, 22, 23, 24, 25, 26, 27, 28].

2.2. Discrete surface model

To obtain the discrete model, we assume that the triangulated lattices, which are embedded in the external space \mathbf{R}^3 , are piecewise linear (PL). The Hamiltonian is

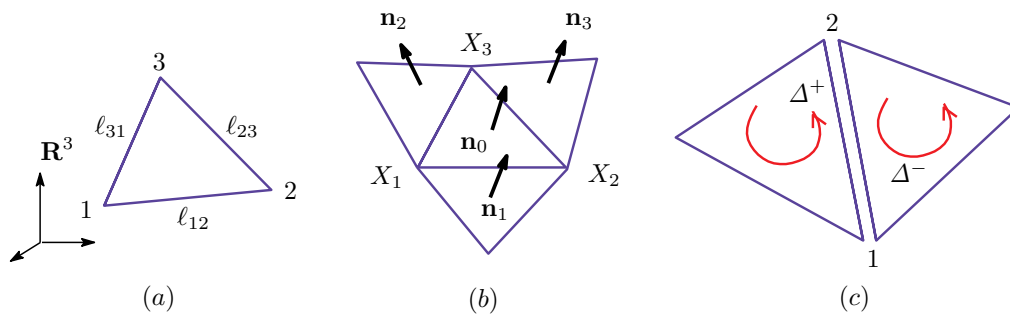


Figure 1. (a) A triangle Δ included in a triangulated sphere in \mathbf{R}^3 , (b) the three nearest neighbor triangles of Δ and the unit normal vectors \mathbf{n}_0 , \mathbf{n}_1 , \mathbf{n}_2 and \mathbf{n}_3 , (c) the triangle orientation which defines the direction-dependent bond potential $\gamma_{12}\ell_{12}^2$ and $\gamma_{21}\ell_{21}^2$ of the bond 12, where $\ell_{12}=\ell_{21}$.

defined on a triangulated lattice which is a PL surface. This PL surface is composed of three simplexes such as vertices, bonds, and triangles. Therefore all physical quantities, including Hamiltonians, and the metric function are defined on those simplexes and in general labeled by integers corresponding to the simplexes. For example, the vertex position X_i is defined at the vertex i , the bond length ℓ_{ij} is defined on the bond ij , and the elements of g_{ab} are defined on the triangle Δ .

We start with the discrete metric g_{ab} such that

$$g_{ab} = \begin{pmatrix} 1/\rho & 0 \\ 0 & \rho \end{pmatrix}, \quad \rho > 0, \quad (2)$$

where ρ is a function on a PL triangle Δ (see Fig. 1(a)). To be more precise, the elements of g_{ab} are functions on the triangle $\Delta_M (\subset M)$, where M is the above mentioned two-dimensional space M (independent of \mathbf{R}^3). We assume that M is also (smoothly) triangulated by the triangles Δ_M . On this Δ_M , an orthogonal coordinate can be taken for any one of three vertices [18]. For this reason, the metric g_{ab} can be diagonalizable, and Δ_M in M is identified with Δ in \mathbf{R}^3 (see Fig. 1(a)) by the mapping X . Therefore, the sentence " ρ is a function on Δ_M " is simply written as " ρ is a function on Δ ". We call this metric in Eq. (2) as discrete metric, because it is defined by the function ρ on the PL triangle Δ . The inequality $\rho > 0$ in Eq. (2) is necessary for the positivity of the bond length, and this g_{ab} makes $ds^2 = g_{ab}dx_a dx_b$ positive definite. This metric depends only on x and is independent of y , and hence it just corresponds to Riemannian metric. Indeed, this metric in Eq. (2) comes from the most general one such as $g_{ab} = \begin{pmatrix} E & F \\ F & G \end{pmatrix}$, with the functions of $E > 0$, $G > 0$, $EG - F^2 > 0$. By assuming $F = 0$, we have $g_{ab} = \begin{pmatrix} E & 0 \\ 0 & G \end{pmatrix} = E \begin{pmatrix} 1 & 0 \\ 0 & G/E \end{pmatrix} \simeq \begin{pmatrix} 1 & 0 \\ 0 & \rho^2 \end{pmatrix} \simeq \begin{pmatrix} 1/\rho & 0 \\ 0 & \rho \end{pmatrix}$, where $\rho^2 = G/E$, and the symbol " \simeq " denotes "conformally equivalent". Note that this expression of g_{ab} depends on the local coordinates on Δ , and therefore the expression of g_{ab} implicitly depends on the vertex of Δ because the coordinate origin is located on one of the vertices

of Δ . In the discrete models that have been studied so far, Euclidean metric $g_{ab} = \delta_{ab}$ is always assumed, and it has been reported that the model for polymerized membranes undergoes a discontinuous transition between the crumpled phase and the smooth phase [29, 30, 31].

Let the vertex X_1 of the central triangle Δ in Fig. 1(b) be the local coordinate origin of this Δ . By replacing

$$\begin{aligned} \int \sqrt{g} d^2x &\rightarrow \sum_{\Delta}, \\ \frac{\partial X^\mu}{\partial x_1} &\rightarrow X_2^\mu - X_1^\mu, \quad \frac{\partial X^\mu}{\partial x_2} \rightarrow X_3^\mu - X_1^\mu, \\ \frac{\partial \mathbf{n}}{\partial x_1} &\rightarrow \mathbf{n}_0 - \mathbf{n}_2, \quad \frac{\partial \mathbf{n}}{\partial x_2} \rightarrow \mathbf{n}_0 - \mathbf{n}_1, \end{aligned} \quad (3)$$

we have

$$\begin{aligned} S_1 &= \sum_{\Delta} S_1(\Delta) = \sum_{\Delta} \left(\rho \ell_{12}^2 + \frac{1}{\rho} \ell_{13}^2 \right), \\ S_2 &= \sum_{\Delta} S_2(\Delta) = \sum_{\Delta} \left[\rho (1 - \mathbf{n}_0 \cdot \mathbf{n}_1) + \frac{1}{\rho} (1 - \mathbf{n}_0 \cdot \mathbf{n}_2) \right], \end{aligned} \quad (4)$$

where $\mathbf{n}_i (i = 1, 2, 3)$ are the unit normal vectors shown in Fig. 1(b). The symbol $\ell_{ij} (= \ell_{ji})$ is defined by $\ell_{ij} = |X_j^\mu - X_i^\mu|$. Note that the unit normal vector also represents the surface orientation, indeed \mathbf{n}_0 is defined by $\mathbf{n}_0 = \vec{\ell}_{12} \times \vec{\ell}_{13} / |\vec{\ell}_{12} \times \vec{\ell}_{13}|$ for example.

We have three possible coordinate origins in the triangles. For this reason, S_1 and S_2 can be symmetrized by including the terms which are cyclic permutations such as $1 \rightarrow 2, 2 \rightarrow 3, 3 \rightarrow 1$ for ℓ_{ij} , \mathbf{n}_i and ρ_i . Multiplying the factor $1/3$, we get

$$\begin{aligned} S_1 &= \frac{1}{3} \sum_{\Delta} \left[\left(\rho_1 + \frac{1}{\rho_2} \right) \ell_{12}^2 + \left(\rho_2 + \frac{1}{\rho_3} \right) \ell_{23}^2 + \left(\rho_3 + \frac{1}{\rho_1} \right) \ell_{31}^2 \right], \\ S_2 &= \frac{1}{3} \sum_{\Delta} \left[\left(\rho_1 + \frac{1}{\rho_2} \right) (1 - \mathbf{n}_0 \cdot \mathbf{n}_1) + \left(\rho_2 + \frac{1}{\rho_3} \right) (1 - \mathbf{n}_0 \cdot \mathbf{n}_3) \right. \\ &\quad \left. + \left(\rho_3 + \frac{1}{\rho_1} \right) (1 - \mathbf{n}_0 \cdot \mathbf{n}_2) \right], \end{aligned} \quad (5)$$

where $\rho_i (i = 1, 2, 3)$ are defined on the triangle Δ . The reason why these three different functions ρ_i are included is because the expression for g_{ab} in general depends on the local coordinate as mentioned above. More precisely, ρ_i is the element of g_{ab} on Δ where the coordinate origin is located at the vertex i . For arbitrary g_{ab} , we always have the metric of the form in Eq. (2) by the same procedure as describe above.

Here we further simplify the model by assuming that

$$\rho_1 = \rho_2 = \rho_3 (= \rho_{\Delta}). \quad (6)$$

Thus, we have the expressions

$$S_1 = \frac{1}{3} \sum_{\Delta} \left(\rho_{\Delta} + \frac{1}{\rho_{\Delta}} \right) (\ell_{12}^2 + \ell_{23}^2 + \ell_{31}^2),$$

$$S_2 = \frac{1}{3} \sum_{\Delta} \left(\rho_{\Delta} + \frac{1}{\rho_{\Delta}} \right) (1 - \mathbf{n}_0 \cdot \mathbf{n}_1 + 1 - \mathbf{n}_0 \cdot \mathbf{n}_2 + 1 - \mathbf{n}_0 \cdot \mathbf{n}_3). \quad (7)$$

Replacing the sum over triangles \sum_{Δ} with the sum over bonds \sum_{ij} , we get

$$\begin{aligned} S_1 &= \frac{2}{3} \sum_{ij} \left(\rho_i + \frac{1}{\rho_i} + \rho_j + \frac{1}{\rho_j} \right) \ell_{ij}^2, \\ S_2 &= \frac{2}{3} \sum_{ij} \left(\rho_i + \frac{1}{\rho_i} + \rho_j + \frac{1}{\rho_j} \right) (1 - \mathbf{n}_i \cdot \mathbf{n}_j). \end{aligned} \quad (8)$$

Note that the suffices i, j of ℓ_{ij} in Eq. (8) denote the bond ij , while those of ρ_i and ρ_j denote the two neighboring triangles i and j of the bond ij . Thus, we finally have

$$\begin{aligned} S(X, \sigma) &= S_1 + \kappa S_2, \\ S_1 &= \sum_{ij} \gamma_{ij} \ell_{ij}^2, \quad S_2 = \sum_{ij} \kappa_{ij} (1 - \mathbf{n}_i \cdot \mathbf{n}_j), \end{aligned} \quad (9)$$

with

$$\gamma_{ij} = \kappa_{ij} = \frac{c_i + c_j}{4}, \quad c_i = \rho_i + \frac{1}{\rho_i}, \quad (10)$$

where the irrelevant numerical factor $2/3$ is replaced by $1/4$ in those final expressions for S_1 and S_2 .

We should note that γ_{ij} (κ_{ij}) can be called effective surface tension (effective bending rigidity) on the bond between the vertices i and j . It must be emphasized that the quantities γ_{ij} and κ_{ij} are independent of the bond direction, or in other words, these are symmetric under the exchange of i and j , and for this reason γ_{ij} and κ_{ij} are considered as the quantities defined on the bond ij . Indeed, from the expression given in Eq. (10), we have

$$\gamma_{ij} = \gamma_{ji}, \quad \kappa_{ij} = \kappa_{ji}. \quad (11)$$

Therefore, the physical quantities $\gamma_{ij} \ell_{ij}^2$ in S_1 and $\kappa_{ij} (1 - \mathbf{n}_i \cdot \mathbf{n}_j)$ in S_2 of Eq. (9) are well defined in the sense that these quantities are symmetric under the exchange of ij . The reason why we need this symmetry in the physical quantities $\gamma_{ij} \ell_{ij}^2$ and $\kappa_{ij} (1 - \mathbf{n}_i \cdot \mathbf{n}_j)$ is because these quantities correspond to the energies for the expansion and bending of the surface at the bond ij , and these energies are independent of the bond direction such as the one from i to j or the reverse. Thus, the symmetry property in Eq. (11) allows us to call γ_{ij} and κ_{ij} respectively the effective surface tension and the effective bending rigidity on the bond ij . We also note that this problem raises only when γ_{ij} and κ_{ij} depend on the functions ρ_i and ρ_j on the two neighboring triangles i and j . This is in sharp contrast to the case where γ_{ij} and κ_{ij} depend only on the quantity defined on the vertices [11], where γ_{ij} and κ_{ij} are always symmetric. This exchange symmetry/asymmetry reflects the orientation symmetry/asymmetry, which will be discussed in the next subsection.

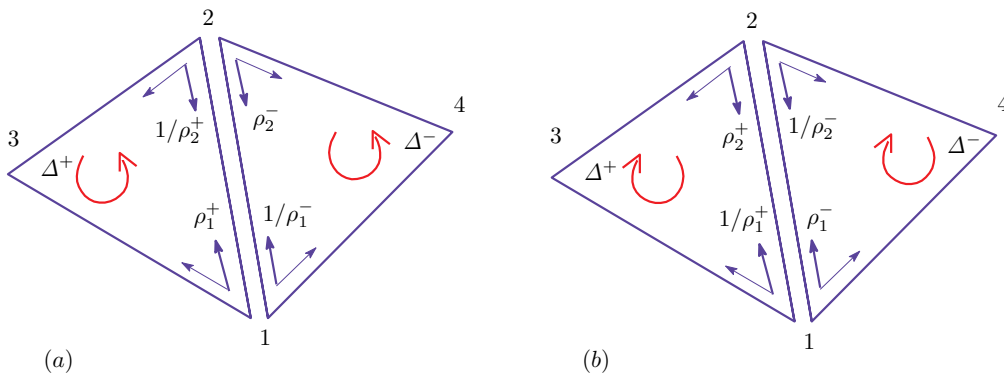


Figure 2. Local coordinate origins of the triangles Δ^+ and Δ^- for $S_1(\ell_{12})$, and the elements of γ_{12} and γ_{21} of the configurations of (a) the original and (b) the inside out (inside view).

2.3. Surface orientation asymmetry and Finsler geometry model

We should remind ourselves of the fact that the symmetry properties in Eq. (11) can be seen in the model only under the condition of Eq. (6). This symmetry is not present in the model of Eq. (5). To see the breakdown of the symmetry of Eq. (11) in the model of Eq. (5) in more detail, we replace the sum over triangles \sum_{Δ} of S_1 and S_2 in Eq. (5) with the sum over bonds \sum_{ij} before the condition of Eq. (6) is imposed. In this new expression of S_1 , which is expressed by the sum over bonds \sum_{ij} , the Gaussian bond potential for the bond 12, which is shared by the triangles Δ_+ and Δ_- as in Fig. 2(a) for example, is given by

$$S_1(\ell_{12}) = (2/3) \left(\rho_1^+ + \frac{1}{\rho_2^+} + \rho_2^- + \frac{1}{\rho_1^-} \right) \ell_{12}^2 \sim \gamma_{12} \ell_{12}^2. \quad (12)$$

In this expression the former half $S_1^+(\ell_{12}) = (2/3) (\rho_1^+ + 1/\rho_2^+) \ell_{12}^2$ is the contribution from Δ_+ , and the latter half $S_1^-(\ell_{12}) = (2/3) (\rho_2^- + 1/\rho_1^-) \ell_{12}^2$ is the one from Δ_- . However, it is clear that γ_{12} and hence $S_1(\ell_{12})$ in Eq. (12) is not symmetric under the change of surface orientation. In fact, we have

$$\bar{S}_1(\ell_{12}) = (2/3) \left(\rho_2^+ + \frac{1}{\rho_1^+} + \rho_1^- + \frac{1}{\rho_2^-} \right) \ell_{12}^2 \sim \gamma_{21} \ell_{12}^2 \quad (13)$$

for the opposite orientation (see Fig. 2(b)). In Eq. (13) we write the coefficient of ℓ_{12}^2 by γ_{21} , because it is obtained by the exchange of 1 and 2 in γ_{12} of Eq. (12). It is easy to see that $\gamma_{12} \neq \gamma_{21}$ and hence $S_1(\ell_{12})$ is not always identical with $\bar{S}_1(\ell_{12})$ in general. Thus, we find that the asymmetry $\gamma_{12} \neq \gamma_{21}$ means that $S_1(\ell_{12})$ is not invariant under the orientation exchange. From this, we can see that the Gaussian bond potential energy (and also the bending energy) of the bond 12 of one surface configuration is different from the one of the opposite orientation configuration. Note that the surface shapes of two configurations are not exactly the same in general, however, they are reflections to each other. This asymmetry between $S_1(\ell_{12})$ and $\bar{S}_1(\ell_{12})$ comes from the fact that $S_1(\ell_{12})^\pm$ are defined by the quantity ρ on the triangles as mentioned above.

Moreover, we have to remark that both the model defined by Eq. (5), which is orientation asymmetric, and the model defined by Eq. (9), which is orientation symmetric, are ill-defined in the context of conventional surface modeling. To see this ill-definedness, it is better to see the relation between the models in Eqs. (5) and (9) in more detail. For this purpose, we impose the following constraints on the model in Eq. (5) such that

$$\begin{aligned}
 \frac{1}{\rho_1^+} + \rho_2^+ &= \frac{1}{\rho_2^-} + \rho_1^-, \\
 \frac{1}{\rho_2^+} + \rho_1^+ &= \frac{1}{\rho_1^-} + \rho_2^-, \\
 \frac{1}{\rho_2^+} + \rho_1^+ + \frac{1}{\rho_1^-} + \rho_2^- &= \frac{1}{\rho_1^+} + \rho_2^+ + \frac{1}{\rho_2^-} + \rho_1^-,
 \end{aligned} \tag{14}$$

where the first two are the constraints that the bond length squares calculated with ρ_i^+ ($i = 1, 2$) in Δ^+ should be identical with the one calculated with ρ_i^- ($i = 1, 2$) in Δ^- in Fig. 2(a). Indeed, the metric on Δ^+ is given by $g_{ab} = \begin{pmatrix} 1/\rho_1^+ & 0 \\ 0 & \rho_1^+ \end{pmatrix}$, where the coordinate origin is at the vertex 1. Then, we have the bond length squares $(1/\rho_1^+) \ell_{12}^2$ for the bond 12, and changing the vertex origin from 1 to 2, we also have $\rho_2^+ \ell_{12}^2$. Thus, summing over these two expressions without the coefficient 1/2, we have $(1/\rho_1^+ + \rho_2^+) \ell_{12}^2$ for the bond length squares. By the same procedure, we have $(1/\rho_2^- + \rho_1^-) \ell_{12}^2$ from Δ^- . Then, equating these two square lengths of the bond 12, we have the first constraint in Eq. (14). Without this constraint, the model is ill-defined in the context of ordinary surface modeling such as HP and Regge on triangulated lattices [34, 35, 36]. In those HP and Regge models, the common understanding is that the edge length of triangles should uniquely be given as the basic requirement even in the discrete models. We should note that the bond "length" used here is the length with respect to g_{ab} on Δ^\pm and is different from the Euclidean bond length ℓ_{ij} . Strictly speaking, this "length" here is the one on Δ_M^\pm in M , where $X(\Delta_M^\pm) = \Delta^\pm$. The bond length consistency should also be required on the triangles in M . The second constraint in Eq. (14) can also be obtained by the same manner from the opposite orientation configuration in Fig. 2(b). Here we note that the coefficients of ℓ_{12}^2 appeared in the calculations of the first and second constraints, where g_{ab} is used, are different from those in $S_1(\ell_{12})$ and $\bar{S}_1(\ell_{12})$ of Eqs. (12), (13), where the inverse g^{ab} is used. The third constraint in Eq. (14) corresponds to $S_1(\ell_{12}) = \bar{S}_1(\ell_{12})$, which comes from the assumption that the Hamiltonian is orientation symmetric. This orientation symmetry should be equipped naively in the model for biological membranes, where the change of orientation can be seen as mentioned in the Introduction. In some of bilayer membrane models, the orientation asymmetry is assumed, and this point will be mentioned later in this subsection.

Here we comment on the relation between the equations in Eq. (14). If the left hand side of the first of Eq. (14) is identical with the left hand side of the second of Eq. (14), the third of Eq. (14) is satisfied, and the converse is not always true. This implies that the bond length squares of a surface is not always identical with the one

of the inverted or buckled surface even when the Gaussian bond potentials of those two surfaces are the same. This is just the case for the model of Eq. (9).

It is easy to see that the solution to those three constraints in Eq. (14) satisfies

$$\rho_1 = \rho_2 (= \rho_\Delta), \quad \frac{1}{\rho_\Delta} + \rho_\Delta = \text{constant}. \quad (15)$$

The first result implies that the functions $\rho_i (i=1, 2, 3)$ on the triangle Δ are expressed by a single function ρ_Δ for example, and hence it corresponds to the assumption in Eq. (6). In the second result in Eq. (15), the "constant" is common for all triangles. We should note that the model defined by Eq. (9) does not always satisfy the second result in Eq. (15), and therefore the model of Eq. (9) does not always satisfy the first two constraints in Eq. (14). However, these two constraints in Eq. (14) are necessary for the conventional surface modeling. Thus, we understand that the model in Eq. (9) is not always well defined. On the other hand, the second result in Eq. (15) is too strong for our purpose, because under this condition we have only constant κ_{ij} and γ_{ij} in Eq. (10). In this case, the phase structure of the model exactly identical with the canonical surface model, where $\kappa_{ij} = \gamma_{ij} = 1$.

Therefore, in a model construction on the triangulated lattices, we always get an ill-defined discrete model if we start with an arbitrary Riemannian metric in which the elements are defined on the triangles. Thus, we have to remark that the model construction described above is logically unsatisfactory. In fact, the model in Eq. (5) is ill-defined because of the bond length inconsistency. Moreover, it is also clear that the model in Eq. (9) is not well-defined because the bond length inconsistency is suspected.

However, those ill-defined models in Eqs. (5) and (9) turn to be well-defined in the context of Finsler geometry. In this context, the first two constraints in Eq. (14) are not necessary, because the bond length calculated with g_{ab} on the triangle Δ^+ can be considered as the Finslerian length of the bond 12 of the direction from 1 to 2, and the one calculated with g_{ab} on Δ^- can be considered as the Finslerian length from 2 to 1. It should also be noted that ℓ_{12} can be called the Euclidean bond length even in the context of Finsler geometry. Moreover, the above mentioned quantities $S_1^+(\ell_{12})$ and $S_1^-(\ell_{12})$ are meaningful in the Finsler geometry context, because these are also considered as direction dependent quantities. The reason is that the metric g_{ab} itself is considered as direction dependent in the sense that it defines the direction dependent inner product of vectors. Indeed, both $S_1^+(\ell_{12})$ and $S_1^-(\ell_{12})$, which are discrete analogue of the continuous S_1 in Eq. (1), are of the form $g^{ab}\ell_a^\mu\ell_b^\mu$ with $\ell_1^\mu = \ell_{12}^\mu$, $\ell_2^\mu = \ell_{13}^\mu$ on the triangle Δ^+ in Fig. 2(a) for example. In this expression, g^{ab} is direction dependent and so is $g^{ab}\ell_a^\mu\ell_b^\mu$. Hence we find that $S_1(\ell_{12})$, which is the sum of these $S_1^+(\ell_{12})$ and $S_1^-(\ell_{12})$, must also be direction dependent. Therefore, we have to remark that both S_1 and S_2 are originally defined to be orientation asymmetric from the Finsler geometric viewpoint. An asymmetric Hamiltonian includes a symmetric one as a special case, however the converse is not true. Thus, the important point to note is that the triangulated and discrete surface model with the Riemannian metric in Eq. (2) is well defined only in the context of Finsler geometry modeling.

The orientation asymmetry is indeed expected in membranes, and this asymmetry has been extensively studied by the area difference bilayer model [37, 38, 39]. Therefore, the orientation asymmetric FG model is meaningful at least for those membranes, although the FG modeling is yet to be done.

Finally in this subsection, we note that the change of surface orientation can be seen by the inversion (or parity transformation) in \mathbf{R}^3 such that

$$X'_1 = -X_1, \quad X'_2 = -X_2, \quad X'_3 = -X_3. \quad (16)$$

It is easy to understand that the surface turns inside out with the opposite surface orientation under this transformation. The change of surface orientation can also be obtained by the reflection such that

$$X'_1 = -X_1, \quad X'_2 = X_2, \quad X'_3 = X_3. \quad (17)$$

These are a linear transformation and not continuous. However, in the inversion or buckling of membranes, only the initial and final configurations are connected to each other by such a discontinuous transformation, and the intermediate states continuously change their shape.

2.4. How to construct Finsler geometry surface model

The outline of the construction of Finsler geometry model is as follows. We emphasize again that the notion of Finsler geometry is necessary for the model in this paper, because without the notion of Finsler geometry the model is problematic or is simply identified with the canonical model. Therefore, we would like to show a technique on how to introduce the model in a logically acceptable manner.

We start with the discrete Finsler function $L(x, y)$ on the triangle Δ [11]:

$$L(x, y) = \begin{cases} y_1/\sqrt{\rho} & (\text{on the } x_1 \text{ axis}), \\ y_2\sqrt{\rho} & (\text{on the } x_2 \text{ axis}), \end{cases} \quad (18)$$

where $y_a = dx_a/dt$ is a tangential vector along the positive direction of the axis x_a [12, 13]. From this function $L(x, y)$ on Δ , we have the bilinear form for the Finsler metric on M such that

$$L_M^2 = \sum_{\Delta} L_{\Delta}^2, \quad L_{\Delta} = \sqrt{y_1^2/\rho + y_2^2\rho}. \quad (19)$$

Using the relation $g_{ab} = (1/2)\partial^2 L_M^2/\partial y_a \partial y_b$, we have $g_{ab} = \begin{pmatrix} 1/\rho & 0 \\ 0 & \rho \end{pmatrix}$, which is the same as the metric in Eq. (2). It is also possible to assume $L_{\Delta} = \sqrt{y_1 + y_2^2\rho^2}$ on Δ .

In this case we have $g_{ab} = \begin{pmatrix} 1 & 0 \\ 0 & \rho^2 \end{pmatrix}$, which is conformally equivalent with the above one. Thus, using the metric g_{ab} obtained from the bilinear form L_M^2 , we have a discrete Hamiltonian $S_1 + \kappa S_2$, where S_1 and S_2 are just the same as those in Eq. (5). We should emphasize that these S_1 and S_2 in Eq. (5) are well-defined even though γ_{ij} and κ_{ij} are

not always symmetric, because we start with the Finsler function of Eq. (19), which is direction dependent. After this stage, the construction procedure is the same as those described below Eq. (5), and we get the model in Eq. (9).

We should note a subtle problem on the difference between g_{ab} in the continuous and discrete models. In the continuous model the above mentioned g_{ab} , given by Eq. (2), is considered as a Riemannian metric because g_{ab} is defined by a function ρ at x on M . Therefore, the length corresponding to this g_{ab} is independent of the direction along an arbitrary line which passes through x , or in other words g_{ab} is symmetric. This is the reason why we write g_{ab} as $g_{ab}(x)$. On the other hand in the discrete model, at the neighborhood of the vertex 1 in Fig. 2 (a) for example, g_{ab} depends on the direction because ρ_Δ is a function on the triangle Δ and $\rho_\Delta \neq \rho_{\Delta'}$ in general. In this sense, g_{ab} in Eq. (2) can be written as $g_{ab}(x, y)$ if it is used as a discrete metric even though $g_{ab}(x, y)$ is not explicitly dependent on y . This is the reason why g_{ab} in Eq. (2) should be understood as the direction dependent metric in the discrete model. Thus, we should understand that $g_{ab}(x, y)$ (and hence $L(x, y)$) is well defined or meaningful only for the positive direction along the curve x , and hence $L(x', y')$ for another curve x' such as the curve of the reverse direction is not always identical with $L(x, y)$ in general. Such a Finsler geometry modeling was applied to a path integral formulation for the quantization of several mechanical systems [32], and it was also pointed out the possibility that the space time manifold is anisotropic and hence it is described by Finsler geometry [33].

From the considerations in this section, it must be emphasized that a triangulated surface model for arbitrary metric function on the triangles is well defined only in the context of Finsler geometry modeling. In other words, even when the continuous surface model is defined with such a Riemannian metric, the corresponding discrete model on triangulated surfaces should be understood in the context of Finsler geometry modeling.

3. Two components surface model

Now, let us introduce a new degree of freedom $\sigma (\in \mathbf{Z}_2 = \{1, -1\})$. We assume that the variable σ_i is defined on the triangle Δ_i , and moreover, the values of σ_i correspond to the two different phases, the liquid ordered (L_o) and the liquid disordered (L_d), such that

$$\sigma(\Delta) = \begin{cases} 1 & (\Delta \in L_o) \\ -1 & (\Delta \in L_d) \end{cases} \quad (20)$$

This definition of σ implies that every triangle is labeled by the value of σ , and therefore σ represents the phase (or domain) to which the triangle Δ belongs.

The total Hamiltonian is given by

$$\begin{aligned} S(X, \sigma) &= \lambda S_0 + S_1 + \kappa S_2, \\ S_0(\sigma) &= \sum_{ij} (1 - \sigma_i \cdot \sigma_j), \end{aligned}$$

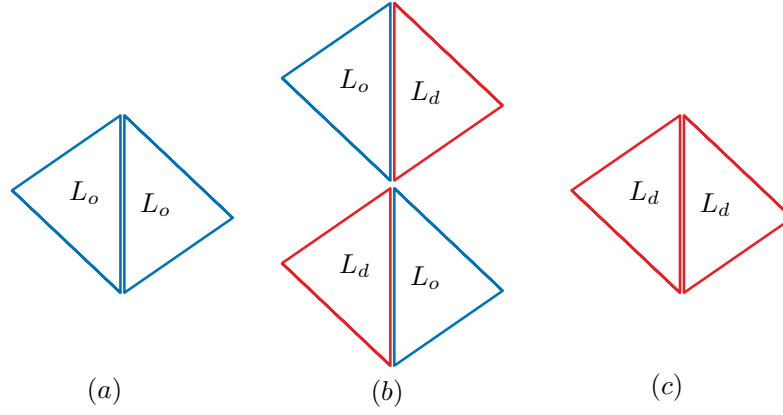


Figure 3. Four possible combinations for the two neighboring triangles. (a) $\kappa_{ij} = \gamma_{ij} = (c + c^{-1})/2$ on the (L_o, L_o) boundary, (b) $\kappa_{ij} = \gamma_{ij} = (2 + c + c^{-1})/4$ on the (L_o, L_d) boundary, and (c) $\kappa_{ij} = \gamma_{ij} = 1$ on the (L_d, L_d) boundary.

$$S_1(X, \sigma) = \sum_{ij} \gamma_{ij}(\sigma) \ell_{ij}^2, \quad S_2(X, \sigma) = \sum_{ij} \kappa_{ij}(\sigma) (1 - \mathbf{n}_i \cdot \mathbf{n}_j), \quad (21)$$

where λS_0 is called *aggregation energy* hence force, S_1 and S_2 are the same as those in Eq. (9). The expressions $\gamma_{ij}(\sigma)$ and $\kappa_{ij}(\sigma)$ denote that γ_{ij} and κ_{ij} depend on the variable σ because of the interaction between σ and X . The interaction between σ and X is defined by the function ρ , which depends on σ such that

$$\rho(\Delta) = \begin{cases} c & (\Delta \in L_o \Leftrightarrow \sigma(\Delta) = 1) \\ 1 & (\Delta \in L_d \Leftrightarrow \sigma(\Delta) = -1), \end{cases} \quad (22)$$

where c is a parameter, which should be fixed at the beginning of the simulations by hand. We should note that we have only $c=1$ if the second of Eq. (15) is assumed.

From this definition of $\rho(\Delta)$ and Eq. (10), we have (see Fig. 3)

$$\gamma_{ij} = \kappa_{ij} = \frac{c_i + c_j}{4} = \begin{cases} (c + c^{-1})/2 & [\sigma_i = \sigma_j = 1 : (L_o, L_o)] \\ (2 + c + c^{-1})/4 & [\sigma_i \sigma_j = -1 : (L_o, L_d)] \\ 1 & [\sigma_i = \sigma_j = -1 : (L_d, L_d)]. \end{cases} \quad (23)$$

These expressions for γ_{ij} and κ_{ij} represent how the effective surface tension γ_{ij} and bending rigidity κ_{ij} depend on the position of the bond ij , which is located in one of the three domain boundaries (L_o, L_o) , (L_o, L_d) , and (L_d, L_d) . Note that only (L_o, L_d) corresponds to the domain boundary and the other two correspond to the bonds inside the domains L_o and L_d . From the expression of γ_{ij} and κ_{ij} in Eq. (23), we understand that the dependence of surface strength on the domains and their boundary is automatically determined in our model. Thus, this expression is one of the most interesting output of the Finsler geometry model in this paper.

In Fig. 4, $\gamma_{ij}(=\kappa_{ij})$ for (L_o, L_o) , (L_o, L_d) , and (L_d, L_d) are plotted as functions of c in the region $1 \leq c$. The expression of γ_{ij} and κ_{ij} in Eq. (23) is symmetric under the exchange $c \leftrightarrow 1/c$, and therefore we use the value of c instead of $1/c$ to represent γ_{ij} and κ_{ij} . The curve of $\gamma_{ij}(=\kappa_{ij})$ against c is almost linear except the region $c \simeq 1$. The

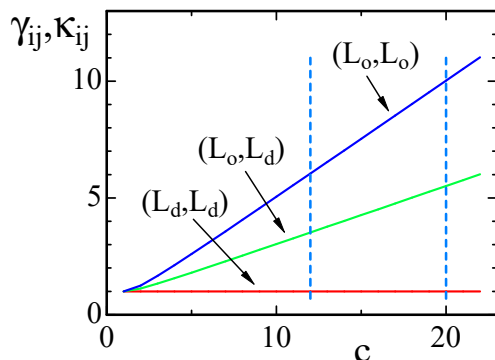


Figure 4. Three different values of γ_{ij} and κ_{ij} vs. c , where $\kappa_{ij} = \gamma_{ij} = (c+c^{-1})/2$ on the (L_o, L_o) boundary, $\kappa_{ij} = \gamma_{ij} = (2+c+c^{-1})/4$ on the (L_o, L_d) boundary, and $\kappa_{ij} = \gamma_{ij} = 1$ on the (L_d, L_d) boundary. The dashed lines denote the values of c assumed in some of the simulations.

dashed vertical lines in the figure correspond $c = 12$ and $c = 20$, which are assumed in the simulations.

The fluid surface model is defined by including the sum over all possible triangulations $\sum_{\mathcal{T}}$ in the partition function such that

$$Z(\lambda, \kappa) = \sum_{\mathcal{T}} \int' \prod_{i=1}^N dX_i \exp[-S(X, \sigma)], \quad (24)$$

where the prime in \int' denotes that the center of mass of the surface is fixed to the origin of \mathbf{R}^3 for the protection of the surface translation [40, 41, 42, 43]. The dynamical triangulation, denoted by $\sum_{\mathcal{T}}$, is performed by the bond flip technique. Due to this bond flip, not only the vertices but also triangles can diffuse freely over the surface.

We should note that the metric variable, or in other words the function ρ , is not summed over (or integrated out) in Z , and hence it is not a dynamical variable. However, the metric variable is effectively considered as dynamical in the sense that ρ changes its value on the surface due to the diffusion of triangles.

It must also be emphasized that the aggregation energy λS_0 just corresponds to the line tension energy in Refs. [3, 4]. Indeed, the energy $1 - \sigma_i \cdot \sigma_j$ at the bond ij has a non-zero positive value only when the bond is on the domain boundary. More precisely, S_0 is proportional to the total number of bonds which form the domain boundary because the mean bond length is constant on the boundary between L_o and L_d . The reason why the mean bond length becomes constant is understood from the scale invariant property of Z in Eq. (24). Indeed, from the scale invariance of Z , we have $\langle S_1 \rangle / N = 3/2$ [24], which means $\langle \gamma_{ij} \ell_{ij}^2 \rangle$ is constant. This implies that $\langle \ell_{ij}^2 \rangle$ and hence $\langle \ell_{ij} \rangle$ becomes constant. This constant depends only on whether the bond ij belongs to L_o , L_d or the boundary between L_o and L_d , because γ_{ij} is constant on those domain and domain boundary as shown in Eq. (23). Note also that the fact that $\langle \ell_{ij}^2 \rangle = \text{constant}$ implies that the mean area of triangles in L_o and that in L_d are respectively constant. Therefore, λS_0 is considered as an extension of the line tension energy, because S_0 is proportional to the

length of the phase boundary if the two phases are clearly separated as the domains L_o and L_d at least.

The remaining problem to be clarified is how the domain boundary is formed and moved on the triangulated surfaces. In experiments, the area fraction of L_o (and L_d) is fixed [3]. Hence, in our model the total number of triangles N_T^o for $\sigma = 1$ (and N_T^d for $\sigma = -1$) is fixed, where the total number of triangles

$$N_T = N_T^o + N_T^d \tag{25}$$

is also fixed to be constant. The relation between the area fraction of L_o and the fraction of N_T^o will be described in the next section. Another constraint imposed on the triangles in our model is that the value of σ_i of the triangle i remains unchanged for all i during the simulations. Therefore, the triangles themselves have to diffuse over the surface to form the domains of L_o and L_d . This triangle diffusion is numerically possible on the dynamically triangulated surfaces, which are called triangulated fluid surfaces, via the Monte Carlo (MC) technique with dynamical triangulation as described above [40, 41, 42, 43].

4. Monte Carlo technique

The canonical Metropolis technique is used [44, 45]. The vertex position X is updated such that $X' = X + \delta X$. The symbol δX denotes a random three-dimensional vector in a sphere of radius R . The new position X' is accepted with the probability $\text{Min}[1, \exp(-\delta S)]$, where $\delta S = S(\text{new}) - S(\text{old})$. The radius R of the small sphere is fixed such that the acceptance rate for the update of X approximately equals 50%.

The triangulation \mathcal{T} is updated by the bond flip technique as described in the previous section [40, 41, 42, 43]. In the bond flip, the two neighboring triangles of the bond change to a new pair of triangles such that the fraction ϕ_0 of L_o (or L_d) remains unchanged, where ϕ_0 is defined by

$$\phi_0 = N_T^o/N_T. \tag{26}$$

More precisely, if the two triangles have the same value of σ before the bond flip, then the new values of σ for the new triangles are fixed to be the same as the old one. On the other hand, if the values of σ are different from each other before the bond flip, then the new values are also fixed randomly to be different. Only by this process, the variable σ is updated. Because of this update of σ through the dynamical triangulation, the function ρ changes and hence a domain structure of L_o (or L_d) is formed on the surface.

We comment on the relation between the fraction ϕ_0 and the area fraction of L_o . As described in the previous section, the mean triangle areas a_o and a_d in the domains L_o and L_d are constant because of the scale invariance of Z . Therefore, the area fraction of L_o can be written as $N_T^o a_o / (N_T^o a_o + N_T^d a_d)$, which is identical with $\phi_0 = N_T^o / N_T$ if $a_o = a_d$. On the other hand, the area fraction of L_o is not always reflected in the fraction ϕ_0 if $a_o \neq a_d$.

The initial configuration for the simulations is fixed to be the random phase, where the L_o (or L_d) phase is randomly distributed on the surface under a constant ratio ϕ_0 . This state corresponds to the two-phase coexistence configuration.

A single Monte Carlo sweep (MCS) consists of N updates of X and N updates for the bond flips. The total number of MCS that should be performed depends on the parameters, however, it ranges approximately from 1×10^8 to 8×10^8 . Almost all MCSs are $2 \times 10^8 \sim 3 \times 10^8$. The simulations at the phase boundaries are relatively time consuming in general, because the domain structures and hence the surface shape change very slowly there. The total number of vertices N is fixed to $N = 5762$ in this paper.

5. Simulation results

Two types of models, which are denoted by model 1 and model 2, are simulated. In model 1, the effective surface tension γ_{ij} is assumed to be $\gamma_{ij} = 1$, and in model 2, no constraint is imposed on both γ_{ij} and κ_{ij} :

$$\begin{aligned} \gamma_{ij} = 1, \quad \kappa_{ij} &= \frac{c_i + c_j}{4}, & (\text{model 1}), \\ \gamma_{ij} = \kappa_{ij} &= \frac{c_i + c_j}{4}, & (\text{model 2}). \end{aligned} \tag{27}$$

The reason why we fix $\gamma_{ij} = 1$ in model 1 is because γ_{ij} influences the surface size from the fact that S_1 in Eq. (21) has the unit of length squares. Indeed, as described in Section 3, from the scale invariance of Z we have $\langle S_1 \rangle / N = 3/2$ [24], and therefore ℓ_{ij}^2 deviates from the constant expected from this relation if the constraint $\gamma_{ij} = 1$ is not imposed on γ_{ij} . Therefore, due to this dependence of ℓ_{ij}^2 on γ_{ij} , the size of triangles in model 2 depends on the domain in which the triangles are included.

The input parameters for the simulations are λ , κ , c , and ϕ_0 , where c is the value of the function ρ in Eq. (22) and determines γ_{ij} and κ_{ij} . The parameter ϕ_0 defined by Eq. (26) is identical with the area fraction in model 1, while it is different from the area fraction in model 2 because the triangle area is not uniform in model 2. More precisely, the mean triangle area in L_o domain is different from that in L_d domain in model 2. In Table 1, we show the parameters assumed in the simulations of which the results are presented below.

5.1. Model 1

We firstly show a phase diagram on the $\lambda - \phi_0$ plane in Fig. 5. The parameters κ and c are fixed to $\kappa = 7$ and $c = 20$ as shown in Table 1, and λ is varied in its relatively small region. We find that in the region $\lambda < 0.1$ the two phases L_o and L_d are not separated, and the domain pattern is at random, and the surface is almost spherical as we see in the snapshots. To the contrary, in the region $\lambda > 0.1$, L_o and L_d are clearly separated, and the two circular domain and the stripe domain appear. The domain structure depends on the value of ϕ_0 , and the corresponding surface morphology appears to be almost

Table 1. The parameters λ , κ and c , which are fixed by hand as the inputs for the simulations, and κ_{ij} is automatically determined by Eq. (27). The symbol * denotes the parameters, which are varied in the simulations.

	λ	κ	c	$\kappa_{ij}(L_o, L_o)$	$\kappa_{ij}(L_o, L_d)$	$\kappa_{ij}(L_d, L_d)$
model 1	*	7	20	10	5.51	1
model 2	*	10	12	6.02	3.51	1
model 2	3	*	20	10	5.51	1

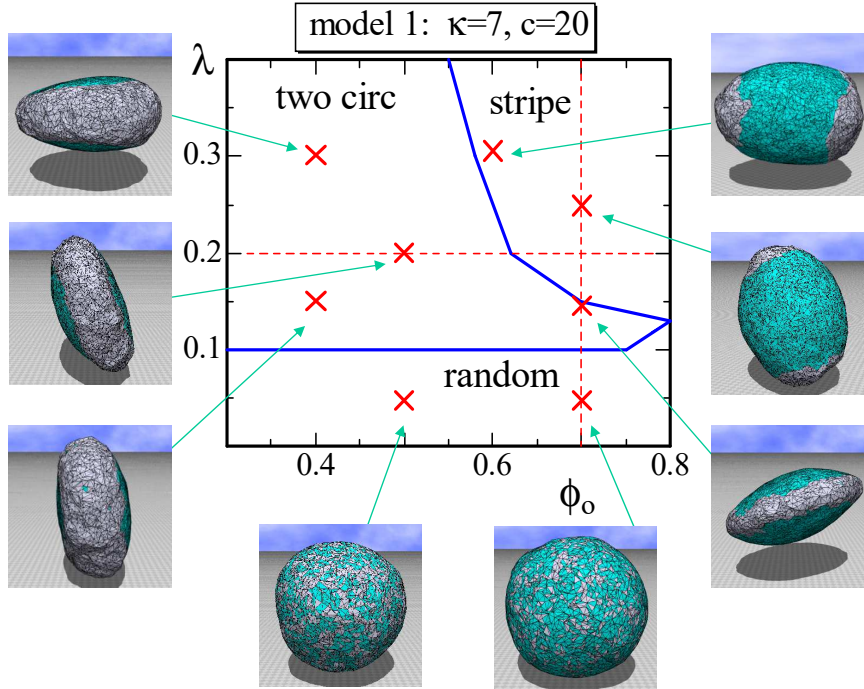


Figure 5. A phase diagram of model 1 on the $\lambda - \phi_o$ plane at $\kappa=7$ and $c=20$, and the snapshots of surfaces obtained at the points indicated by the symbol (\times). The solid lines denote the phase boundaries, and the dashed lines denote the positions for the simulations for Figs. 7 (a),(b)

discontinuously separated on the phase diagram. We see that the two circulars domain changes to the stripe domain as the fraction ϕ_o , which is identical with the area fraction of L_o , increases for constant λ . This is consistent with the experimental results reported in [3], where the area fraction of L_o is changed. The two circulars domain and the stripe domain correspond to the L_o phase, where κ_{ij} is higher than those of both the L_d domain and the boundary as shown in Table 1. For this reason, the L_o domain is relatively smooth compared with the L_d domain. The ratio $\kappa_{ij}(L_o, L_o)/\kappa_{ij}(L_d, L_d)(= 6 \sim 10)$ assumed in the simulations is comparable to or slightly larger than the experimental prediction $\kappa_{ij}(L_o, L_o)/\kappa_{ij}(L_d, L_d)(=1 \sim 4)$ [3].

Next, to show the dependence of surface size on the parameters, we define three diameters D_1 , D_2 , and D_3 of the surface such that $D_1 > D_2 > D_3$ as in Fig. 6.

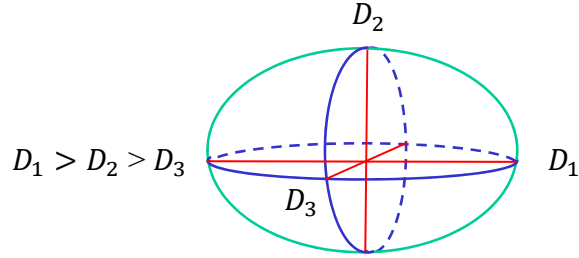


Figure 6. The surface size is characterized by three diameters D_1 , D_2 , and D_3 , where $D_1 > D_2 > D_3$. The three axes are perpendicular to each other.

Numerically, we firstly find the axis for D_1 such that it passes through the center of mass of the surface and the radius D_1 is maximal. Then the axis for D_2 is found on the surface section, which is at the center of the first axis and perpendicular to the first axis, such that D_2 becomes the maximal diameter of the section. Finally we find the axis for D_3 such that it is perpendicular to the first and second axes.

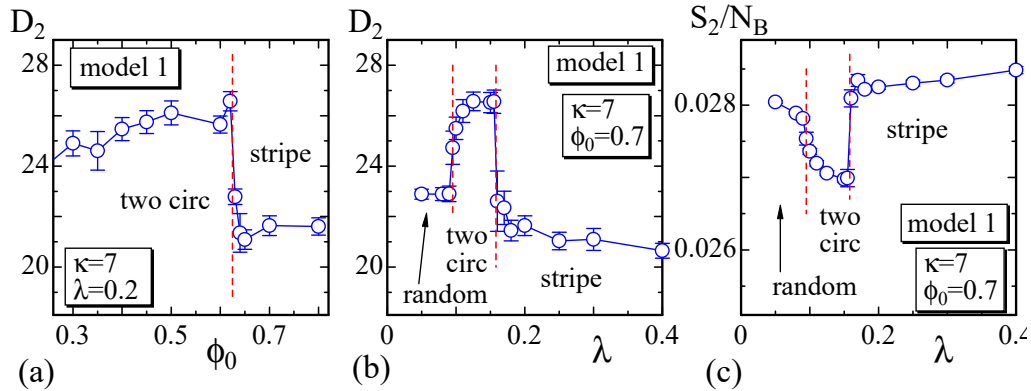


Figure 7. (a) The size D_2 vs. ϕ_0 at $\lambda = 0.2$, (b) D_2 vs. λ at $\phi_0 = 0.7$, and (c) the bending energy S_2/N_B vs. λ at $\phi_0 = 0.7$. These are calculated on the dashed horizontal and vertical lines in Fig. 5. The size D_2 and the bending energy S_2/N_B change almost discontinuously and smoothly at the phase boundaries, which are denoted by the vertical dashed lines.

We plot the second longest diameter D_2 vs. ϕ_0 in Fig. 7(a), where $\lambda = 0.2$. We see that D_2 discontinuously changes against ϕ_0 at the phase boundary between the two circulars and stripe domains. From the plot of D_2 vs. λ in Fig. 7(b), we also see that D_2 discontinuously changes at the same phase boundary. The bending energy S_2/N_B in Fig. 7(c) also discontinuously changes at this boundary, and this indicates that this morphological change is considered as a first order transition. However, we have to note that the change of the morphology at this phase boundary is not always so sharp. In fact, one circular domain surface, which is not shown as a snapshot in Fig. 5, can be seen at the boundary. This implies that the stripe domain surface and one circulars domain surface have the same bending energy, or in other words, the bending energy is degenerate. Note also that the phase boundary between the two circulars and random domains appears to be continuous. This means that the shape of the two circulars

domain surface continuously changes to the random domain surface. At this phase boundary, the surface shape continuously changes from pancake to sphere.

5.2. Model 2

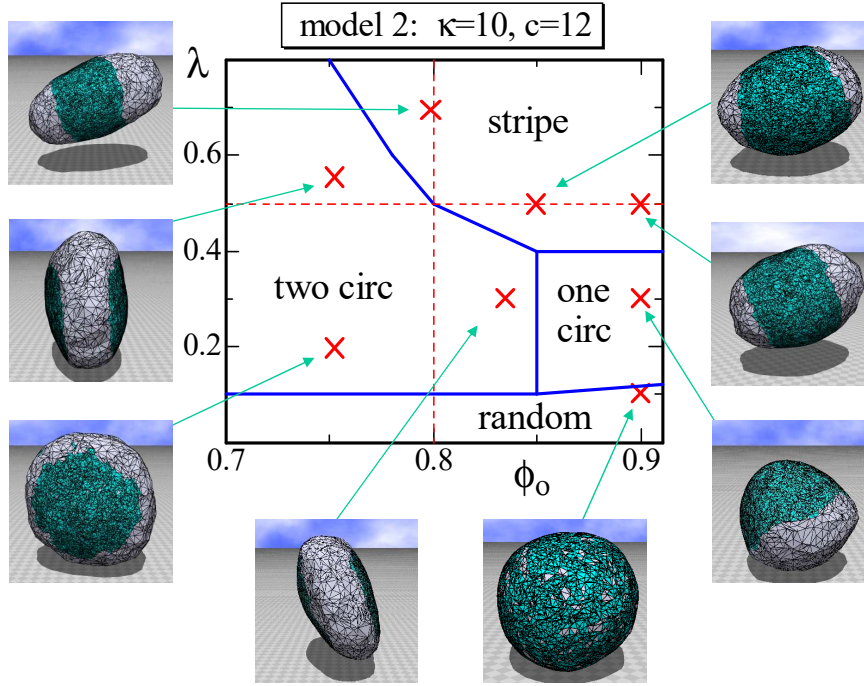


Figure 8. A phase diagram of model 2 on the $\lambda - \phi_o$ plane at $\kappa = 10$ and $c = 12$, and the snapshots of surfaces. The solid lines on the phase diagram denote the phase boundaries, and the dashed lines denote the positions for the simulations for Figs. 9 (a),(b)

In model 2, not only κ_{ij} but also γ_{ij} depends on the domain (or the domain boundary) whether it is L_o or L_d . For this reason, the area of triangles in the L_o domain becomes much smaller than that of the L_d domain. Therefore, the fraction ϕ_o does not reflect the area fraction of L_o in this case. In fact, it is easy to see that the area fraction of L_o in the snapshots at $\phi_o = 0.9$ in Fig. 8 is much smaller than 90%. Nevertheless, the phase diagram on the $\lambda - \phi_o$ plane in Fig. 8 looks almost the same as that in Fig. 5. Only difference between the two phase diagrams is the appearance of one circular domain phase denoted by "one circ" in Fig. 8. This one circular phase is stable, where "stable" means the surface domain remains unchanged against a small variation of the parameters inside the phase boundary. This is in sharp contrast to the one circular domain surfaces seen at the region close to the boundary between the two circulars and stripe domains, because those one circular surfaces are very sensitive to the parameter variation and hence "unstable". The shape of the one circular surface in the one circular region is almost spherical as the one shown in Fig. 8, and this is in contrast to the result in Ref. [4], where the one circular phase is separated

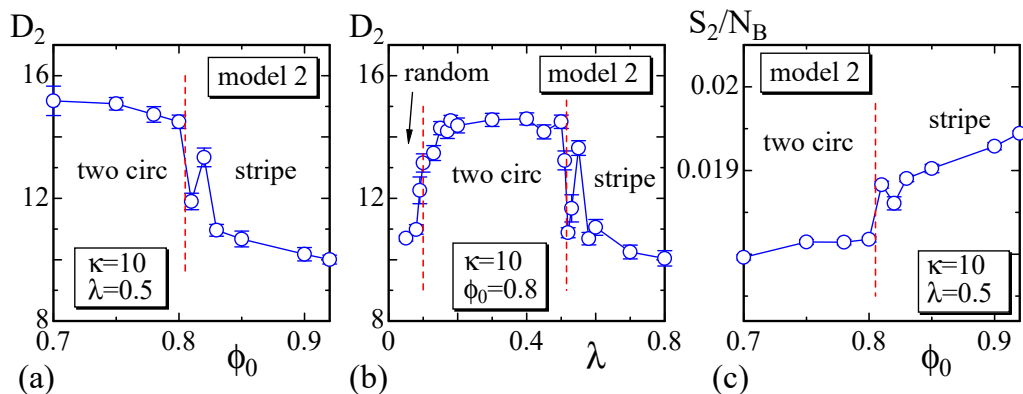


Figure 9. (a) The size D_2 vs. ϕ_0 at $\lambda=0.5$, (b) D_2 vs. λ at $\phi_0=0.8$, and (c) the bending energy S_2/N_B vs. ϕ_0 at $\lambda=0.5$. These are calculated on the dashed horizontal and vertical lines in Fig. 8. The size of the surface changes almost discontinuously and smoothly at the phase boundaries, which are denoted by the dashed lines.

into two phases the prolate and oblate phases. One possible reason why only spherical surface appears in the one circular domain in Fig. 8 is because the L_o domain is hardly bend due to the high ratio $\kappa_{ij}(L_o, L_o)/\kappa_{ij}(L_d, L_d) = 6.02$, which is larger than the one $1 < \kappa_{ij}(L_o, L_o)/\kappa_{ij}(L_d, L_d) < 3$ assumed in Ref. [4]. The parameters assumed on this plane are $\kappa=10$ and $c=12$, which are listed in Table 1.

The simulations are also performed on the $\lambda - \phi_0$ planes for larger κ such as $\kappa=15$ and $\kappa=20$, and with $c=12$. The phase diagrams obtained in those simulations are (not shown) relatively close to the one in Fig. 8, however the surfaces with three or four circulars domain appear in the lower λ region in the two circulars domain phase. The bending energy κS_2 of the three or four domains is lower than that of the two circulars domain, moreover the aggregation energy λS_0 of those multi circular domains is larger than that of the two circulars domain. These are the reason for the appearance of the three or four domains only in the relatively small λ region in those simulations with relatively large κ .

To see the variation of the surface size at the phase boundaries, we calculate the size D_2 on the dashed lines in Fig. 8 and plot them in Figs. 9(a), (b). We find that D_2 discontinuously changes against ϕ_0 and λ at the phase boundaries just like in model 1 shown in Figs. 7(a), (b). Moreover, the phase boundary is also not so clear because of the same reason as that for model 1. In fact, the surface shape at the phase boundary between the two circulars and stripe domains is not always stable in model 2 just like in model 1. We also see from Fig. 9(c) that S_2/N_B discontinuously changes, however the gap is very small, and hence that these two phases are separated by a weak first order transition. The phase boundary between the two circulars and the random domains is also expected to be continuous in model 2. The boundaries of one circular to two circulars and one circular to stripe are also not so clear, and the boundary of one circular to random is continuous.

Another difference between model 1 and model 2, other than the appearance of the

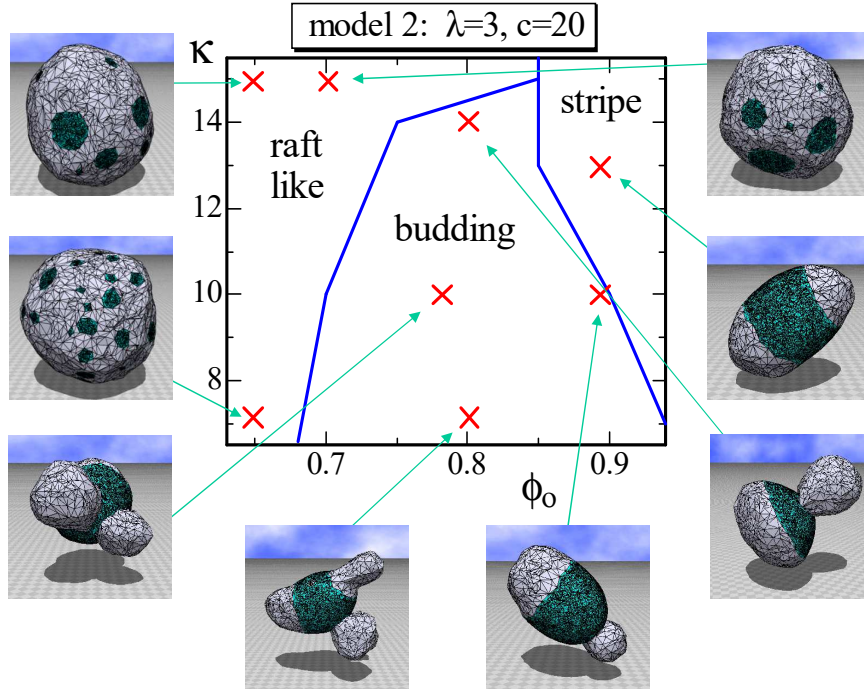


Figure 10. A phase diagram of model 2 on the $\kappa - \phi_0$ plane at $\lambda = 3$ and $c = 20$, and the snapshots of surfaces. The solid lines on the phase diagram denote the phase boundaries.

stable one circular domain, is the raft like domain and the budding domain. To be more precise, the budding domain can also be seen in model 1, however, it is more clear in model 2. The phase diagram of model 2 on the $\kappa - \phi_0$ plane is drawn in Fig. 10. The parameter λ is fixed to $\lambda = 3$, which is relatively large compared with the previous one assumed in the simulations for Figs. 5 and 8. As a consequence, the energy λS_0 , which is the line tension energy, at the phase boundary between L_o and L_d , becomes large in the region where κ is relatively small. This is the reason why the budding domain appears on this $\kappa - \phi_0$ plane in Fig. 10. We should note that the budding domain in some of the budding surfaces goes inside the surface and some of them self-intersect because no self-avoiding interaction is assumed. We also see in Fig. 10 that the raft like domain is stable at relatively large κ region, where the surface hardly deforms. The reason why the raft domains, which are multi circular domains, appear only at the region of small ϕ_0 is because the multi circular domains are energetically favorable than the stripe domain. Indeed, the effective bending rigidity $\kappa \kappa_{ij}$ and hence κS_2 becomes very large on the large connected L_o domain such as the stripe domain, where the line tension energy λS_0 is relatively small. Note that S_0 has non-zero positive value only on the boundary bonds between L_o and L_d , while S_2 has non-zero value on all of the bonds. Note also that the boundary length between L_o and L_d becomes longer (shorter) if the total number of circular domains increases (decreases), while the areas of L_o and L_d remain constant and are independent of this total number.

6. Summary and conclusion

We have studied the phase separation of the three-component membrane with DPPC, DOPC, and Cholesterol using a Finsler geometry (FG) surface model. The results obtained by MC simulations are consistent with the experimental ones that have been reported in the literatures. The FG model is obtained by replacing the surface metric g_{ab} with a Finsler metric in the ordinary Helfrich-Polyakov (HP) model for membranes. This new model includes a new degree of freedom σ , which represents the liquid ordered (L_o) and liquid disordered (L_d) domains. From the Monte Carlo data, we find the phase separation of L_o and L_d domains on the surface, and that the surface shows a variety of morphologies such as the two circulars domain, the stripe domain, the raft domain, and the budding. These morphological changes have been understood by the line tension energy included in the conventional HP model Hamiltonian. We have emphasized that this line tension energy just corresponds to the aggregation energy term λS_0 in our model, because the value of S_0 is nothing else than the total number of bonds on the boundary between L_o and L_d . Moreover, the fact that λS_0 is just the line tension energy implies that the line tension originates from the interaction between the domains. This interaction is closely connected to the property of the new model that the surface strength, such as the surface tension and the bending rigidity, are dependent on the bond position on the surface. This property comes from the interaction between σ and X introduced via the Finsler metric.

As described in Section 2, the Hamiltonian of general FG surface model is sensitive to orientation asymmetric surfaces. Therefore, it is interesting to study FG model as a model for membranes in more general situations including the case with the broken orientation symmetry such that the energy is different for two surfaces which transform to each other by the inversion or reflections.

Acknowledgment

We acknowledge Hideo Sekino, Andrey Shobukhov, and Giancarlo Jug for discussions. This work is supported in part by JSPS KAKENNHI Number 26390138.

References

- [1] Sarah L. Veatch and Sarah L. Keller, Miscibility Phase Diagrams of Giant Vesicles Containing Sphingomyelin, *Phys. Rev. Lett.* **94** (2005) 148101.
- [2] Miho Yanagisawa, Masayuki Imai, and Takashi Taniguchi, Shape Deformation of Ternary Vesicles Coupled with Phase Separation, *Phys. Rev. Lett.* **100** (2008) 148102.
- [3] Miho Yanagisawa, Masayuki Imai, and Takashi Taniguchi, Periodic modulation of tubular vesicles induced by phase separation, *Phys. Rev. E* **82** (2010) 051928.
- [4] Erwin Gutleiderer, Thomas Gruhn and Reinhard Lipowsky, Polymorphism of vesicles with multi-domain patterns, *Soft Matter*, **5** (2009) 3303.
- [5] Prank Jülicher and Reinhard Lipowsky, Domain-induced budding of vesicles, *Phys. Rev. Lett.* **70** (1993) 2964.
- [6] Prank Jülicher and Reinhard Lipowsky, Shape transformations of vesicles with intramembrane domains, *Phys. Rev. E* **53** (1996) 2670.

- [7] Giancarlo Jug, Theory of the thermal magnetocapacitance of multicomponent silicate glasses at low temperature, *Philos. Mag.* **84** (33), (2004) 3599.
- [8] A.M. Polyakov, Quantum geometry of bosonic strings, *Quantum geometry of fermionic strings*, *Phys. Lett. B* **103** (1981) 207, 211.
- [9] A.M. Polyakov, Fine structure of strings, *Nucl. Phys. B* **268** (1986) 406.
- [10] W. Helfrich, Elastic Properties of Lipid Bilayers: Theory and Possible Experiments, *Z. Naturforsch* **28c** (1973) 693.
- [11] H. Koibuchi and H. Sekino, Monte Carlo studies of a Finsler geometric surface model, *Physica A* **393** (2014) 37.
- [12] M. Matsumoto, *Keiryō Bibun Kikagaku* (in Japanese), (Shokabo, Tokyo, 1975).
- [13] D. Bao, S.-S. Chern, Z. Shen, *An Introduction to Riemann-Finsler Geometry*, GTM 200 (Springer, New York, 2000).
- [14] Stephanie Höhn, Aurelia R. Honerkamp-Smith, Pierre A. Haas, Philipp Khuc Trong, and Raymond E. Goldstein, Dynamics of a Volvox Embryo Turning Itself Inside Out, *Phys. Rev. Lett.* **114** (2015) 178101.
- [15] Lenz M, Crow DJG, Joanny JF, Membrane Buckling Induced by Curved Filaments, *Phys. Rev. Lett.* **103** (2009) 038101.
- [16] T. Hamada, H. Hagihara, M. Morita, Mun'delanji C. Vestergaard, Y. Tsujino, and M. Takagi, *J. Phys. Chem. Lett.* **3** (2012) 430.
- [17] Akihiko Saitoh, Kingo Taniguchi, Yohko Tanaka, and Hirokazu Hotani, *Proc. Natl. Acad. Sci.* **95** (1998) 1026.
- [18] F. David, Geometry and Field Theory of Random Surfaces and Membranes, in *Statistical Mechanics of Membranes and Surfaces, Second Edition*, eds. D. Nelson, T. Piran, and S. Weinberg, (World Scientific, Singapore, 2004) p.140.
- [19] Y. Nambu, Duality and Hadrodynamics, in *Broken symmetry, Selected Papers of Y. Nambu*, eds. T. Eguchi and K. Nishijima, (World Scientific, Singapore, 1995) p.280.
- [20] M. Paczusi, M. Kardar and D.R. Nelson, Landau Theory of the Crumpling Transition, *Phys. Rev. Lett.* **60**, (1988) 2638.
- [21] Y. Kantor and D.R. Nelson, Phase transitions in flexible polymeric surfaces, *Phys. Rev. A* **36** (1987) 4020.
- [22] L. Peliti and S. Leibler, Effects of Thermal Fluctuations on Systems with Small Surface Tension, *Phys. Rev. Lett.* **54** (1985) 1690.
- [23] F. David and E. Guitter, Crumpling Transition in Elastic Membranes: Renormalization Group Treatment, *Europhys. Lett.* **5** (1988) 709.
- [24] J.F. Wheeler, Random surfaces: from polymer membranes to strings, *J. Phys. A Math. Gen.* **27** (1994) 3323.
- [25] D. Nelson, The Statistical Mechanics of Membranes and Interfaces, in *Statistical Mechanics of Membranes and Surfaces, Second Edition*, eds. D. Nelson, T. Piran, and S. Weinberg, (World Scientific, Singapore, 2004) p.1.
- [26] M. Bowick and A. Travesset, The statistical mechanics of membranes, *Phys. Rep.* **344** (2001) 255.
- [27] K.J. Wiese, Polymerized Membranes, a Review, in *Phase Transitions and Critical Phenomena 19*, eds. C. Domb, and J.L. Lebowitz (Academic Press, London, 2000) p.253.
- [28] G. Gompper and D.M. Kroll, Triangulated-surface models of fluctuating membranes, in *Statistical Mechanics of Membranes and Surfaces, Second Edition*, eds. D. Nelson, T. Piran, and S. Weinberg, (World Scientific, Singapore, 2004) p.359.
- [29] J-P. Kownacki and H. T. Diep, First-order transition of tethered membranes in three-dimensional space, *Phys. Rev. E* **66** (2002) 066105.
- [30] J.-P. Kownacki and D. Mouhanna, Crumpling transition and flat phase of polymerized phantom membranes, *Phys. Rev. E.* **79** (2009) 040101.
- [31] K. Essafi, J.-P. Kownacki, and D. Mouhanna, First-order phase transitions in polymerized phantom membranes, *Phys. Rev. E* **89** (2014) 042101.

- [32] T. Ootsuka and E. Tanaka, Finsler geometrical path integral, *Phys. Lett. A* **374** (2010) 1917.
- [33] G.Yu. Bogoslovsky and H.F. Goenner, On the possibility of phase transitions in the geometric structure of space-time, *Phys. Lett. A* **244** (1998) 222.
- [34] T. Regge, General Relativity without Coordinates, *Nuovo Cim.* **19** (1961) 558.
- [35] H. W. Hamber, Simplicial Quantum Gravity, in *Critical Phenomena, Random Systems, Gauge Theories*, Proc. of the Les Houches Summer School 1984, eds. K. Osterwalder and R. Stora, (North-Holland, 1986) p.375.
- [36] F. David, Simplicial Quantum Gravity and Random Lattices, Les Houches lecture 1992, arXiv:hep-th/9303127.
- [37] Udo Seifert, Karin Berndl, and Reinhard Lipowsky, Shape transformations of vesicles: Phase diagram for spontaneous-curvature and bilayer-coupling models, *Phys. Rev. A* **44** (1991) 1182.
- [38] K. Berndl, J. Käs, R. Lipowsky, E. Sackmann and U. Seifert, Shape Transformations of Giant Vesicles: Extreme Sensitivity to Bilayer Asymmetry, *Europhys. Lett.* **13** (1990) 659.
- [39] Ling Miao, Udo Seifert, Michael Wortis, and Hans-Günther Döbereiner, Budding transitions of fluid-bilayer vesicles: The effect of area-difference elasticity, *Phys. Rev. E* **49** (1996) 5389.
- [40] A. Baumgärtner and J.-S. Ho, Crumpling of fluid vesicles, *Phys. Rev. A* **41** (1990) 5747(R).
- [41] S.M. Catterall, Extrinsic curvature in dynamically triangulated random surfaces, *Phys. Lett. B* **220** (1989) 207.
- [42] S.M. Catterall, J.B. Kogut, and R.L. Renken, Numerical study of field theories coupled to 2D quantum gravity, *Nucl. Phys. B Proc. Suppl.* **25** (1992) 69.
- [43] J. Ambjörn, A. Irbäck, J. Jurkiewicz, B. Petersson, The theory of dynamical random surfaces with extrinsic curvature, *Nucl. Phys. B* **393** (1993) 571.
- [44] N. Metropolis, A. W. Rosenbluth, M. N. Rosenbluth and A. H. Teller, Equation of State Calculations by Fast Computing Machines, *J. Chem. Phys.* **21** (1953) 1087.
- [45] D.P. Landau, Finite-size behavior of the Ising square lattice, *Phys. Rev. B* **13** (1976) 2997.